Chinese Chemical Letters 34 (2023) 108234

Contents lists available at ScienceDirect

Chinese Chemical Letters

journal homepage: www.elsevier.com/locate/cclet

Black phosphorus nanosheets-based tumor microenvironment responsive multifunctional nanosystem for highly efficient photo-/sono-synergistic therapy of non-Hodgkin lymphoma

Xueli Zhu[a,1], Shengmin Zhang[a,1], Yi Cao[b,c], Xiaojiao Ge[b], Yi Huang[a], Feng Mao[a], Bo Chen[b], Juan Li[b,*], Youfeng Xu[a,*], Aiguo Wu[b,*]

[a] Department of Ultrasound, Central Laboratory, Ningbo First Hospital, Ningbo 315000, China
[b] Cixi Institute of Biomedical Engineering, International Cooperation Base of Biomedical Materials Technology and Application, Chinese Academy of Sciences (CAS) Key Laboratory of Magnetic Materials and Devices, Zhejiang Engineering Research Center for Biomedical Materials, Ningbo Institute of Materials Technology and Engineering, CAS, Ningbo 315201, China
[c] University of Chinese Academy of Sciences, Beijing 100049, China

ARTICLE INFO

Article history:
Received 12 November 2022
Revised 14 February 2023
Accepted 15 February 2023
Available online 18 February 2023

Keywords:
Non-Hodgkin's lymphoma
Black phosphorus
IR780
Phototherapy
Sonodynamic therapy

ABSTRACT

Finding improved therapeutic protocols against non-Hodgkin's lymphoma (NHL) remains an unmet clinical demand. Phototherapy is a promising alternative treatment for traditional clinical therapeutic methods, but the limited tissue penetration blocks the therapeutics. Inspired by the excellent physical and chemical properties of black phosphorus nanosheets (BPNSs), a fluorescence and thermal imaging guided photo-/sono-synergistic treatment platform BPNSs@PEG-SS-IR780/RGD is developed. This ingenious multifunctional theranostic platform not only exhibits outstanding photothermal conversion efficiency and highly efficient reactive oxygen species generation, but also has good biocompatibility, tumor-targeting and tumor microenvironment responsiveness. In addition, BPNSs@PEG-SS-IR780/RGD could actively target the tumor sites and generate excellent photothermal, photodynamic and sonodynamic therapeutic efficacy. Both *in vitro* and *in vivo* experiments indicate that BPNSs@PEG-SS-IR780/RGD can be a promising nanomaterial for NHL imaging and therapy. Taken together, this study not only expands the application field of black phosphorus materials, but also provides a possibility to design a new generation of NHL treatment regimens with clinical application potential.

Non-Hodgkin's lymphoma (NHL) is a primary malignant disease that occurs worldwide [1–3]. Unlike other malignant tumors, lymphomas can affect any organ and tissues throughout the body, presenting as multiple lesions, and it is also prone to relapse [1,4]. Currently, conventional treatments for NHL include chemotherapy, radiotherapy and immunotherapy etc. Although the remission rate of certain aggressive NHL has been reached, the efficacy of regular treatment is very limited for relapses and refractory NHL [1,5]. Therefore, an efficient, non-invasive treatment method for NHL is urgently needed in clinic.

With unique advantages of highly efficient, minimally invasive, low side effects and systemic toxicity, phototherapy is becoming a promising alternative and supplement for traditional tumor treatment [6,7]. However, phototherapy has its inherent drawbacks, for instance, the photon intensity decreases obviously with the increase of tissue depth. Moreover, the photo generated heat distribution in tumor tissues is uneven during phototherapy, and the severe hypoxia environment inside the tumor also results in the poor efficacy. Therefore, a single treatment cannot eradicate tumors, especially those in deep tissue [8,9].

Sonodynamic therapy (SDT) is a non-invasive treatment based on low-frequency ultrasound, in which ultrasound activates an acoustic sensitizer to produce reactive oxygen species (ROS) and induces tumor cell death through apoptosis and/or necrosis [10,11]. As ultrasound has a good penetration ability for soft tissue, it can accurately position and produce good therapeutic effects on deep tumors. Therefore, the combination of photo-/sono-therapy might provide a new strategy for the NHL treatment. However, the sensitizers could be used for both photo-/sono-therapy are quite limited [6,8].

* Corresponding authors.
E-mail addresses: lij@nimte.ac.cn (J. Li), xuyoufeng2017@163.com (Y. Xu), aiguo@nimte.ac.cn (A. Wu).
[1] These authors contributed equally to this work.

https://doi.org/10.1016/j.cclet.2023.108234
1001-8417/

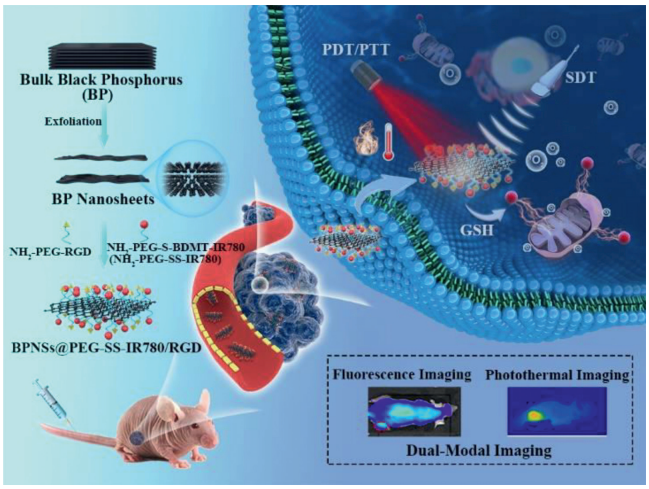

Scheme 1. Schematic illustration of the BPNSs@PEG-SS-IR780/RGD preparation and its application as fluorescence and photothermal imaging-guided phototherapy and sonodynamic synergistic therapy.

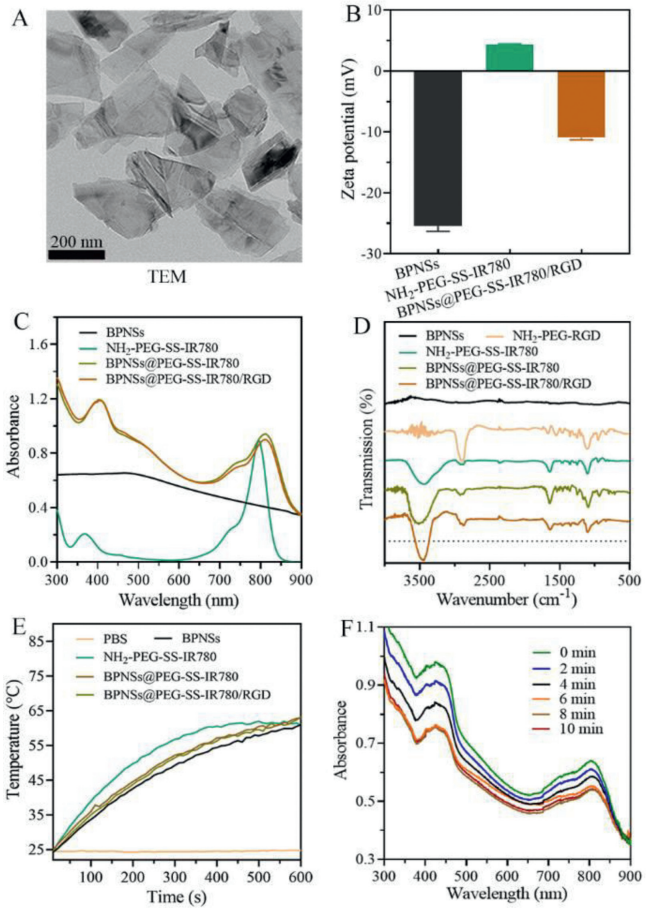

Fig. 1. (A) TEM image, (B) zeta potential (mV) of bare BPNSs, NH_2-PEG-SS-IR780, and BPNSs@PEG-SS-IR780/RGD. (C) UV-vis-NIR spectra, (D) FT-IR spectrum, (E) photothermal heating curves of samples. (F) Sonodynamic therapy performance of BPNSs@PEG-SS-IR780/RGD under an ultrasound irradiation (1.0 MHz, 1.0 W/cm^2, 50% duty cycle).

In recent years, black phosphorus nanosheets (BPNSs) have attracted great interest in biomedical science due to its high surface area, outstanding biocompatibility, and good biodegradability [12–15]. BPNSs-based nanomaterial has become a new multifunctional theranostic platform with broad application prospects due to its unique characteristics. After irradiation with laser, BPNSs can produce obvious photothermal effects, and also has a certain role as photodynamic and sonodynamic sensitizer [16–19]. Dong *et al.* have combined PEGylated BPNSs with Ce6 as an imaging guided photothermal/photodynamic cancer therapy platform, which can be a promising nanotheranostic agent [20]. On the other hand, as a piezoelectric material, Yang and co-workers also use BPNSs as a sonodynamic sensitizer to safely ablate tumors [18]. However, BPNSs electrostatic adsorption small molecule fluorescent dyes directly will lead to fluorescence quenching [20], and the selection of targeting ligand also plays a very important role in rational design and preparation of novel anticancer drugs [21].

Thus, a novel multifunctional theranostic nanoplatform combining BPNSs and heptamethine cyanine dye IR780 and targeted molecule RGD has been designed in this work (Scheme 1). This BPNSs@PEG-SS-IR780/RGD nanoplatform was prepared by electrostatically adsorbing positively charged water-soluble NH_2-PEG-S-BDMT-IR780 (NH_2-PEG-SS-IR780) and NH_2-PEG-RGD on the surface of the BPNSs. In this construction, BPNSs not only serve as carrier, but also is a photothermal and sonodynamic sensitizer; NH_2-PEG-RGD serve as the targeting section, helping to actively target the tumor area; The disulfide bonds in NH_2-PEG-SS-IR780 can release IR780 in the tumor environment, avoiding the fluorescence quenching of the loaded IR780. Furthermore, the NH_2-PEG-RGD and NH_2-PEG-SS-IR780 also can be used to improve the stability of the BPNSs [22–24]. IR780 not only have the photothermal and fluorescence imaging capabilities, but also can serve as the sensitizer for photo-/sono-therapy. This strategy does not only endow the theranostic nanoplatform with the capacity of effective targeting and responsive release in tumor environment, but also possesses strong fluorescence emission, photo-/sono-therapy capability. To the best of our knowledge, it is the first time that the phototherapy combined with sonodynamic therapy used for the NHL research, and the BPNS-based platform has not served as the sensitizer for photo-/sono-synergistic therapy before.

Firstly, the NH_2-PEG-SS-IR780 was synthesized (Fig. S1 in Supporting information) and the high-resolution mass spectrometry was used to characterize its structure with satisfactory result (Figs. S2 and S3 in Supporting information). On the other hand, the BPNSs were prepared with a liquid exfoliation method [12,25]. Transmission electron microscopy (TEM) and atomic force microscopy (AFM) were used to observe the morphology of BPNSs. The TEM image displayed that the lateral size of BPNSs was around 200 nm (Fig. 1A) and the lattice fringes of the BPNSs. The thickness of BPNSs was measured to be less than 10 nm by AFM images (Fig. S4 in Supporting information). The chemical composition of BPNSs was validated by X-ray photoelectron spectroscopy (XPS) analysis (Fig. S5A in Supporting information), The XPS pattern that exhibited the peaks at 129.5 and 130.4 eV were referred to the P $2p_{3/2}$ and P $2p_{1/2}$ orbitals in the P 2p spectrum, respectively. Oxidized phosphorus signal (*i.e.*, PxOy) caused by slight degradation of BPNSs appears as a low peak near 133 eV as previously reported [26]. From X-ray diffractometry (XRD), BPNSs could be indexed into orthorhombic crystal structure consistent with the standard JCPDS card No. 73-1358 (Fig. S5B in Supporting information). Furthermore, the Raman spectra were used to verify the structure of BPNSs (Fig. S5C in Supporting information). The peaks located at 356.9, 430.6 and 456.9 cm^{-1}, correspond to A_{1g}, B_{2g}, and A_{2g} modes of BP, respectively, manifested that the structure of exfoliated BPNSs was not affected comparing with bulk counterparts.

After being adsorbed with NH_2-PEG-RGD and NH_2-PEG-SS-IR780, the average lateral size almost remains constant. The size distribution detected by dynamic light scattering (DLS) revealed that BPNSs and BPNSs@PEG-SS-IR780/RGD were 190.9 ± 75.2 nm

and 195.9 ± 70.3 nm, respectively (Fig. S6 in Supporting information). The zeta potential of BPNSs@PEG-SS-IR780/RGD increased from −25.4 ± 0.9 mV to −10.9 ± 0.4 mV comparing with bare BPNSs (Fig. 1B). The successful loading of NH_2-PEG-RGD and NH_2-PEG-SS-IR780 onto BPNSs was testified by UV-visible spectrophotometer (UV-vis), fourier transform infrared spectroscopy (FT-IR), and fluorescence spectrometer. BPNSs exhibited a broad absorption band proportional to the concentration spanning from UV to NIR region. BPNSs@PEG-SS-IR780/RGD in PBS demonstrated a new absorption peak around 780 nm compared to BPNSs, refers to the characteristic band for IR780 (Fig. 1C). The structures of the products were also characterized by FT-IR (Fig. 1D). With absorption bands at 2700-3000 cm^{-1} and 880-1700 cm^{-1}, which were attributable to the PEG segment, the coating of NH_2-PEG-RGD and NH_2-PEG-SS-IR780 was confirmed. The fluorescence spectra demonstrated that the fluorescence peak of BPNSs@PEG-SS-IR780/RGD was at 803 nm, confirming the successful loading of NH_2-PEG-SS-IR780 (Fig. S7 in Supporting information). The loading behavior of BPNSs with NH_2-PEG-SS-IR780 was also investigated. Different ratios of NH_2-PEG-SS-IR780 were added into BPNSs suspension, with the concentration ratio of IR780 to BPNSs was 2, 4, 6, 8 and 10, respectively. After removing superfluous free NH_2-PEG-SS-IR780, the obtained BPNSs@PEG-SS-IR780 was measured by UV-vis spectra, and the loading capacities of NH_2-PEG-SS-IR780 were shown in Fig. S8 (Supporting information). Once increasing the concentration ratio of NH_2-PEG-SS-IR780/BPNSs, the loading capacity is nonlinearly increased, which may be due to the large specific surface area of BPNSs.

To evaluate the photothermal property of BPNSs@PEG-SS-IR780/RGD, the temperature changes were investigated by a thermal imaging camera to record the photothermal curves and images. Fig. 1E and Fig. S9 (Supporting information) demonstrated that the temperature rises were 36.7, 36.5, 38.3 and 38.3 °C for BPNSs, NH_2-PEG-SS-IR780, BPNSs@PEG-SS-IR780, BPNSs@PEG-SS-IR780/RGD, respectively after 10 min laser irradiation (660 nm) with the power density of 0.6 W/cm^2. The temperature of BPNSs@PEG-SS-IR780/RGD could dramatically reach 63.3 °C, after being irradiated for 10 min at a relatively low concentration, which contains 25 μg/mL BPNSs and 11.5 μg/mL IR780. As depicted in Fig. S10 (Supporting information), the temperature of BPNSs (25 μg/mL) increased by 25.5 and 36.7 °C at the power density of 0.45 and 0.6 W/cm^2, respectively, indicating BPNSs displayed power density- and concentration-dependent temperature variation behavior. Additionally, the photothermal conversion efficiency (η) of BPNSs and NH_2-PEG-SS-IR780 was calculated to be 40.7% and 37.2%, respectively (Fig. S11 in Supporting information), demonstrating the excellent photothermal effect of BPNSs and IR780. As displayed in Fig. S12 (Supporting information), even after five on/off irradiation cycles with a 660 nm laser (0.6 W/cm^2), BPNSs can also keep a stable photothermal effect, revealing satisfactory photostability, while PEG-SS-IR780 degraded quickly during the first two cycling processes.

ROS generation performance is the key factor to estimate SDT and PDT properties of nanomaterials [7], so 1,3-diphenylisobenzofuran (DPBF) was taken as the probe to evaluate the ROS generation. As illustrated in Figs. S13A-C (Supporting information), there were almost no changes in absorbance was observed for BPNSs group after irradiated under 660 nm laser, even the laser power density reached 0.6 W/cm^2. However, after being treated with the ultrasound, the absorbance intensity of the BPNSs at peak 410 nm dropped gradually corresponding to the power density and time, suggesting a good ROS generation capacity (Figs. S14A and B in Supporting information). As for NH_2-PEG-SS-IR780, the absorbance dropped quickly both at peak 410 and 780 nm throughout the 660 nm laser or ultrasound irradiation process (Figs. S13D-F, S14C and D in Supporting information). This phenomenon indicates that although IR780 has an excellent ROS yield, it still can be rapidly degraded under the laser and ultrasonic irradiation. As shown in Fig. 1F, BPNSs@PEG-SS-IR780/RGD also exhibited a good ROS performance under ultrasonic irradiation, while the decomposition of IR780 was not obvious.

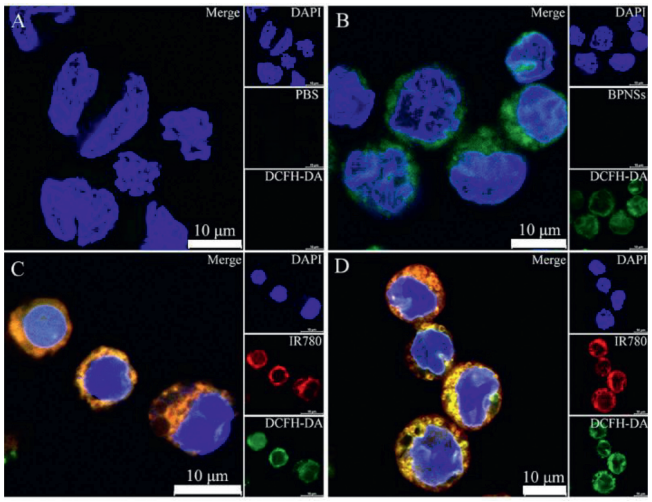

Fig. 2. *In vitro* cellular uptake and ROS generation of (A) PBS, (B) BPNSs, (C) BPNSs@PEG-SS-IR780, (D) BPNSs@PEG-SS-IR780/RGD *via* confocal fluorescence imaging. Intracellular ROS generation of Raji cells treated with above-mentioned different samples and irradiated with ultrasound and 660 nm laser (Green: DCFH-DA as ROS probe; Blue: nuclear were stained with DAPI; Red: IR780).

In vitro cellular uptake and ROS generation properties of BPNSs@PEG-SS-IR780/RGD were investigated by confocal fluorescence imaging. After incubation with NH_2-PEG-SS-IR780, BPNSs@PEG-SS-IR780 and BPNSs@PEG-SS-IR780/RGD for 4 h, human Burkitt's lymphoma cells Raji demonstrated obvious red fluorescence in cytoplasm, indicating excellent cellular uptake of those three samples (Fig. 2 and Fig. S15 in Supporting information). 2,7-Dichlorodihydrofluorescein diacetate (DCFH-DA) was used as a ROS probe, which can react with ROS to produce green fluorescence to evaluate the intracellular SDT and PDT performance of nanomaterials. When Raji cells were only cultured with BPNSs, there were only weak green fluorescence in cytoplasm after the 660 nm laser exposure, but more obvious green fluorescence was observed after ultrasound exposure (Fig. S16 in Supporting information), indicating that the intracellular ROS generation properties of SDT is better than that of PDT. When Raji cells were cultured with NH_2-PEG-SS-IR780, BPNSs@PEG-SS-IR780 or BPNSs@PEG-SS-IR780/RGD irradiated with 660 nm laser or/and ultrasound, the cytoplasm exhibits abundant bright green fluorescence, verifying robust ROS generation performance *in vitro* (Fig. 2 and Fig. S15).

In vitro cell viability and photo-/sono-therapeutic effects of BPNSs@PEG-SS-IR780/RGD were demonstrated by cell counting kit-8 (CCK-8) assay and Calcein-AM/PI. For the cells intervened with BPNSs, NH_2-PEG-SS-IR780, BPNSs@PEG-SS-IR780 or BPNSs@PEG-SS-IR780/RGD without laser and ultrasound irradiation, cell survival rates were still more than 75%, even the concentration of BPNSs or IR780 is high up to 50 μg/mL (Fig. 3A). After laser (660 nm, 0.6 W/cm^2, 5 min) and ultrasound irradiation (1.0 MHz, 1.0 W/cm^2, 30 s), 39% of Raji cells were alive after being treated with BPNSs@PEG-SS-IR780/RGD (BPNSs: 12.5 μg/mL, IR780: 5.5 μg/mL), which was much lower than that of being irradiated by the laser (62%) or ultrasound alone (73%). The therapeutic effects of BPNSs@PEG-SS-IR780/RGD further enhanced with increasing concentration, and almost all Raji cells were killed when the concentration reached 50 μg/mL under laser and ultrasound irradiation (Fig. 3B). Overall, the combination of BPNSs@PEG-SS-IR780/RGD

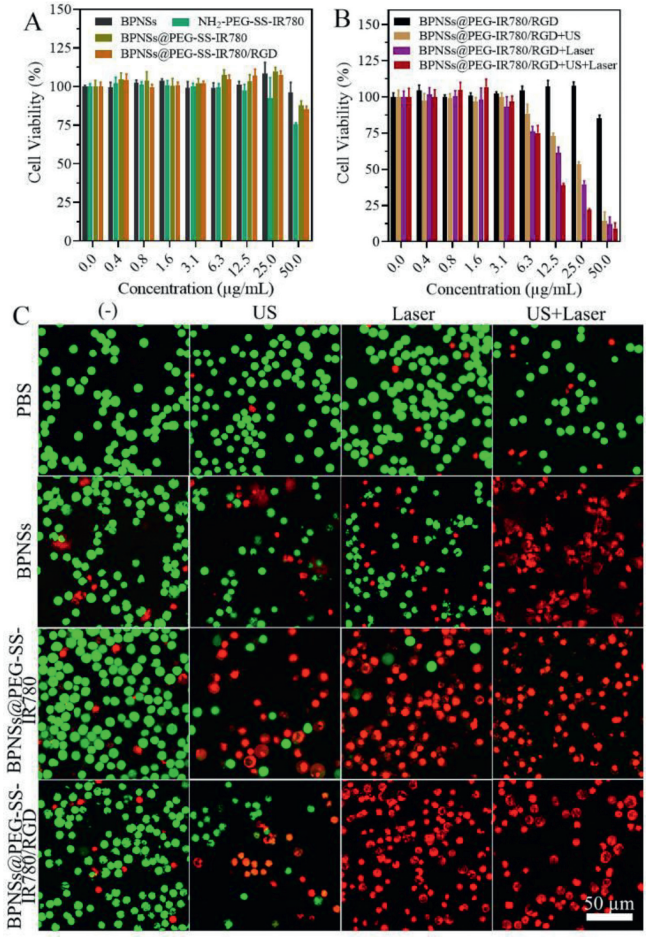

Fig. 3. Relative viabilities of Raji cells after treated with different samples at different concentrations: (A) without or (B) with the irradiation of laser and US (the relative viabilities of Raji cells cultured with different concentrations of BPNSs@PEG-SS-IR780/RGD). (C) Fluorescence images of Raji cells stained with Calcein AM (green fluorescence, live cells) and PI (red fluorescence, dead cells) after various treatments. Laser: 660 nm, 0.6 W/cm^2, 5 min; US: 1.0 MHz, 1.0 W/cm^2, 50% duty cycle, 30 s.

with both ultrasound and laser irradiation shows the outstanding cytotoxicity superior to the combination with ultrasound or laser alone. As we know, calcein AM can be hydrolyzed by endogenous esterases to emit green fluorescence in living cells, while propidium iodide (PI) can bind with the nuclear DNA of apoptosis or dead cells with strong red fluorescence emission. The therapeutic effects of BPNSs@PEG-SS-IR780/RGD were further verified by the Calcein AM/PI. As illustrated in Fig. 3C, almost all the cells cultured with BPNSs@PEG-SS-IR780/RGD were dead after the US and laser irradiation, while a high cell viability was observed when only introducing BPNSs, BPNSs@PEG-SS-IR780, and BPNSs@PEG-SS-IR780/RGD. Taken together, the results of CCK-8 and Calcein AM/PI tests both confirmed the advantage of photo-/sono-synergistic cancer therapy.

Encouraged by the promising anticancer efficacy of synergistic therapy *in vitro*, the *in vivo* applications of BPNSs@PEG-SS-IR780/RGD was further evaluated, and all performances of *in vivo* experiments followed the guidelines and regulations of Care and Use of Laboratory Animals of Ningbo University and approved by the Animal Ethics Committee of Animal Experiments at Ningbo University (Permit No. SYXK (Zhe) 2019-0005). Firstly, the biosafety of nanomaterials was investigated on ICR mice, and no mice died during the 14 days observation period after the tail intravenous injection of PBS, BPNSs, BPNSs@PEG-SS-IR780 and BPNSs@PEG-SS-IR780/RGD, respectively. At day 14, all mice were euthanized for blood and main organs (heart, liver, spleen, lung, and kidney) were collected. The results of blood routine analysis and serum biochemistry assay did not differ significantly among tested groups (Fig. S17 in Supporting information). Furthermore, histological analysis revealed that there was no evident damage to the main organs of mice in each group (Fig. S18 in Supporting information). All these results indicated that the BPNSs@PEG-SS-IR780/RGD has excellent biocompatibility and was tolerable by mice.

The fluorescence and thermal dual imaging were further conducted by using BPNSs@PEG-SS-IR780/RGD on Raji-bearing BALB/c nude mice. After tail intravenous injection of BPNSs@PEG-SS-IR780 and BPNSs@PEG-SS-IR780/RGD, fluorescence imaging was performed to monitor the dynamic fluorescence change to explore the *in vivo* distribution and tumor accumulation of these nanomaterials. As displayed by Fig. 4A, the fluorescence signal of the BPNSs@PEG-SS-IR780 and BPNSs@PEG-SS-IR780/RGD could be observed at the tumor sites at 6 h post-injection, and gradually increases until 72 h after injection. Compared with the BPNSs@PEG-SS-IR780, BPNSs@PEG-SS-IR780/RGD was more likely to accumulate at tumor location through RGD active targeting and enhanced permeability and retention (EPR) passive targeting effect. The *ex vivo* fluorescence images of tumor and organs resected at 72 h post-injection were showed in Fig. S19 (Supporting information). As for the BPNSs@PEG-SS-IR780/RGD group, more strong fluorescence could be observed in the tumor site, also elucidating better tumor targeting capacity than BPNSs@PEG-SS-IR780. The biodistribution of BPNSs@PEG-SS-IR780 and BPNSs@PEG-SS-IR780/RGD was quantified by the parameter of average radiant efficiency (Fig. 4B and Fig. S20 in Supporting information), and displayed the same results as the fluorescence imaging.

In addition, a thermal imaging camera was used to monitor the temperature at the tumor location under 660 nm laser irradiation. The representative temperature curve at the tumor site of different groups were shown in Fig. 4D. The temperature of mice treated with BPNSs@PEG-SS-IR780/RGD increased about 20 °C within 10 min irradiation, which might be due to the efficient tumor accumulation and the robust photothermal property of BPNSs@PEG-SS-IR780/RGD. In the PBS group, by contrast, the temperature variation at the tumor site after laser irradiation was almost negligible. The corresponding thermal images evidently displayed the changes of temperature at the tumor site (Fig. 4C). Consequently, the dual-modal of BPNSs@PEG-SS-IR780/RGD would provide precise guidance during tumor treatment process.

To further verify the antitumor efficacy of BPNSs@PEG-SS-IR780/RGD, Raji-bearing mice were randomized divided into 10 groups for different treatments: PBS, BPNSs, BPNSs@PEG-SS-IR780 and BPNSs@PEG-SS-IR780 with or without laser or ultrasound irradiation. After 24 h caudal vein injection of different agents, the tumor sites of the mice in the predetermined groups were exposed to 660 nm laser (0.6 W/cm^2) and/or ultrasound (1.0 MHz, 1.0 W/cm^2, 50% duty cycle) for 10 min, respectively. After being treated, the tumor volume and body weight of all groups were recorded every other day for 14 days and standardized with their initial values (0 day). All groups of mice experienced a slow increase in body weight and no mice died during the treatment period (Fig. 4E). As illustrated in Fig. 4F, PBS, PBS + Laser + US, BPNSs, BPNSs@PEG-SS-IR780, and BPNSs@PEG-SS-IR780/RGD all experienced rapid tumor growth during the treatment period, indicating very limited therapeutic effect. However, tumor volumes increased slowly for BPNSs + Laser + US, BPNSs@PEG-SS-IR780 + Laser + US, BPNSs@PEG-SS-IR780/RGD + US, and BPNSs@PEG-SS-IR780/RGD + Laser group, indicating the tumor growth was inhibited effectively. Excitingly, BPNSs@PEG-SS-IR780/RGD + Laser + US group displayed the most excellent tumor ablation effect, which is in accordance with that of the *in vitro* synergistic anticancer efficacy. After 14 days, blood routine

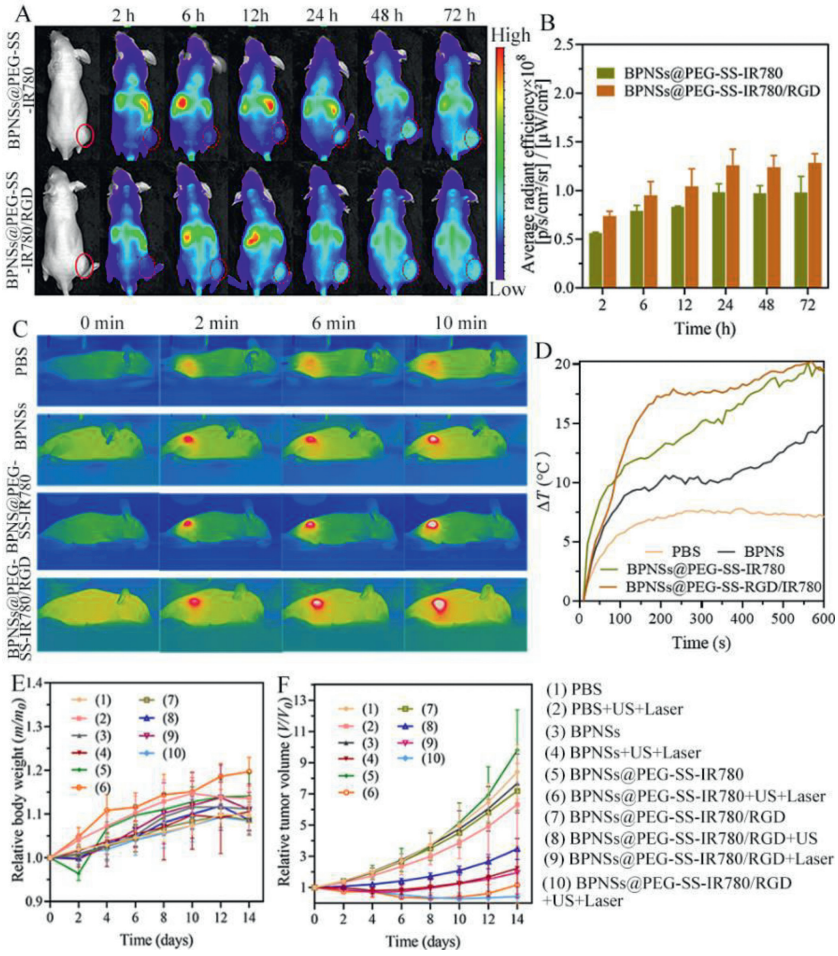

Fig. 4. *In vivo* fluorescence imaging, thermal performance and antitumor study on Raji-tumor-bearing mice. (A) fluorescence images of mice bearing Raji tumors after injection of BPNSs@PEG-SS-IR780 or BPNSs@PEG-SS-IR780/RGD, and (B) the corresponding fluorescence intensity of tumor site changing with time *in vivo* was quantified by average radiant efficiency. (C) Thermal images of tumor-bearing mice after injection of different samples followed by irradiation with a 660 nm laser (0.6 W/cm^2, 10 min), the temperature curves of tumor sites during laser irradiation as displayed in (D). (E) The body weights of mice were monitored every other day during the anti-tumor therapy period. (F) Relative tumor growth curves in different groups of mice treated in different protocols. The relative tumor volumes were normalized to their initial sizes.

and serum biochemistry assay were performed for BPNSs@PEG-SS-IR780/RGD + Laser + US group, the measured indexes showed no significant difference between tested group and PBS group (Fig. S21 in Supporting information). Furthermore, the major organs (heart, liver, spleen, lung, and kidney) were harvested and stained with H&E for pathological analysis, the images of H&E staining displayed that there was no observed damage of the major organs (Fig. S22 in Supporting information), further confirming the favorable biocompatibility of BPNSs@PEG-SS-IR780/RGD, and this synergistic therapy was tolerable by mice. Additionally, the proliferative and apoptotic activity of tumors cells after photo-/sono-synergistic treatment with BPNSs@PEG-SS-IR780/RGD was assessed by H&E and immunohistochemical staining assay. As illustrated in Fig. S23 (Supporting information), the most obvious apoptosis or necrosis of tumor cells were shown in the group of synergistic therapy, and the proliferative cells were sporadically visible in tumor tissue. These results verified that the BPNSs@PEG-SS-IR780/RGD can effectively kill tumor cells and inhibit their proliferation by synergistically treatment.

In summary, this tumor microenvironment responsive BPNSs-based multifunctional nanosystem has been successfully developed. The prepared BPNSs@PEG-SS-IR780/RGD with excellent stability and biocompatibility exhibits good tumor-targeting property, efficiently ROS yield, good photothermal conversion efficiency and strong fluorescence. The presented hybrid nanoplatform demonstrates a remarkably enhanced antitumor efficacy through photo-/sono-synergistic treatment in *in vitro* and *in vivo* experiment, presenting a great potential for precise NHL imaging and therapy. The successful application of this novel tumor microenvironment sensitive multimodal platform may provide new possibility in developing next generation of multifunctional nanomaterials for cancer treatment.

Declaration of competing interest

The authors declare that they have no known competing financial interests or personal relationships that could have appeared to influence the work reported in this paper.

Acknowledgments

This work was financially supported by the National Natural Science Foundation of China (Nos. 31971292, 81871411, 32011530115 and 32111540257), the Science & Technology Bureau of Ningbo City (Nos. 2020Z094, 2021Z072, 2021J269), and Ningbo Health Youth Technical Key Talents Training Project (No. rc2021011).

Supplementary materials

Supplementary material associated with this article can be found, in the online version, at doi:10.1016/j.cclet.2023.108234.

References

[1] J.O. Armitage, R.D. Gascoyne, M.A. Lunning, F. Cavalli, The Lancet 390 (2017) 298–310.
[2] R.L. Siegel, K.D. Miller, H.E. Fuchs, A. Jemal, CA Cancer J. Clin. 71 (2021) 7–33.
[3] H. Sung, J. Ferlay, R.L. Siegel, et al., CA Cancer J. Clin. 71 (2021) 209–249.
[4] A. Bowzyk Al-Naeeb, T. Ajithkumar, S. Behan, D.J. Hodson, BMJ 362 (2018) k3204.
[5] K.M. Au, A. Tripathy, C.P. Lin, et al., ACS. Nano 12 (2018) 1544–1563.
[6] S. Son, J.H. Kim, X. Wang, et al., Chem. Soc. Rev. 49 (2020) 3244–3261.
[7] X. Lin, J. Song, X. Chen, H. Yang, Angew. Chem. Int. Ed. 59 (2020) 14212–14233.
[8] W. Yue, L. Chen, L. Yu, et al., Nat. Commun. 10 (2019) 2025.
[9] X. Pan, W. Wang, Z. Huang, et al., Angew. Chem. Int. Ed. 59 (2020) 13557–13561.
[10] Z. Gong, Z. Dai, Adv. Sci. (Weinh) 8 (2021) 2002178.
[11] S. Liang, X. Deng, P. Ma, Z. Cheng, J. Lin, Adv. Mater. 32 (2020) e2003214.
[12] M. Qiu, W.X. Ren, T. Jeong, et al., Chem. Soc. Rev. 47 (2018) 5588–5601.
[13] W. Chen, J. Ouyang, X. Yi, et al., Adv. Mater. 30 (2018) e1703458.
[14] S. Anju, J. Ashtami, P.V. Mohanan, Mater. Sci. Eng. C: Mater. Biol Appl. 97 (2019) 978–993.
[15] X. Liang, X. Ye, C. Wang, et al., J. Control. Release 296 (2019) 150–161.
[16] B. Li, C. Lai, G. Zeng, et al., Small 15 (2019) e1804565.
[17] J. Liu, P. Du, T. Liu, et al., Biomaterials 192 (2019) 179–188.
[18] Z. Li, T. Zhang, F. Fan, et al., J. Phys. Chem. Lett. 11 (2020) 1228–1238.
[19] T. Chen, W. Zeng, C. Tie, et al., Bioact. Mater. 10 (2022) 515–525.
[20] X. Yang, D. Wang, Y. Shi, et al., ACS. Appl. Mater. Interfaces 10 (2018) 12431–12440.
[21] K.R. Gajbhiye, V. Gajbhiye, I.A. Siddiqui, J.M. Gajbhiye, J. Drug Target 27 (2019) 111–124.
[22] Z. Shi, Q. Li, L. Mei, Chin. Chem. Lett. 31 (2020) 1345–1356.
[23] M. Ou, C. Lin, Y. Wang, et al., J. Control. Release 345 (2022) 755–769.
[24] X. Zeng, M. Luo, G. Liu, et al., Adv. Sci. (Weinh) 5 (2018) 1800510.
[25] J.N. Coleman, M. Lotya, A. O'Neill, et al., Science 331 (2011) 568–571.
[26] J. Huang, B. He, Z. Zhang, et al., Adv. Mater. 32 (2020) e2003382.